

# An Experimental and Theoretical Approach to Understanding the Surface Properties of One-Dimensional TiO<sub>2</sub> Nanomaterials

Atiđa Selmani,<sup>\*,†</sup> Mario Špadina,<sup>†</sup> Milivoj Plodinec,<sup>‡</sup> Ida Delač Marion,<sup>§</sup> Marc Georg Willinger,<sup>||</sup> Johannes Lützenkirchen,<sup>⊥</sup> Harry D. Gafney,<sup>#</sup> and Engelbert Redel<sup>\*,∇</sup>

<sup>†</sup>Department of Chemistry, Faculty of Science, University of Zagreb, Horvatovac 102a, 10002 Zagreb, Croatia

<sup>‡</sup>Department of Material Physics, Ruđer Bošković Institute, Bijenička 54, 10000 Zagreb, Croatia

<sup>§</sup>Institute of Physics, Bijenička 46, Zagreb, Croatia

<sup>||</sup>Department of Inorganic Chemistry, Fritz Haber – Institute of the Max Planck Society, Faradayweg 4-6, D-14195 Berlin, Germany

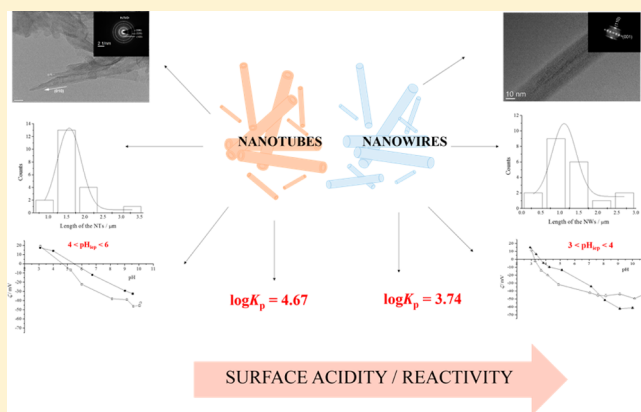
<sup>⊥</sup>Institut für Nukleare Entsorgung (INE), Karlsruher Institut für Technologie (KIT), Postfach 3640, 76021 Karlsruhe, Germany

<sup>#</sup>Department of Chemistry, Queens College, City University of New York, Flushing, New York 11367, United States

<sup>∇</sup>Karlsruhe Institute of Technology (KIT), Institute of Functional Interfaces (IFG), Hermann-von-Helmholtz-Platz 1, D-76344, Eggenstein-Leopoldshafen, Germany

## S Supporting Information

**ABSTRACT:** The present research focuses on the comparative investigation of the acid–base surface properties (the isoelectric point,  $\text{pH}_{\text{iep}}$  and point of zero charge,  $\text{pH}_{\text{pzc}}$ ) of one-dimensional TiO<sub>2</sub> nanomaterials. Different one-dimensional TiO<sub>2</sub> nanomaterials, nanotubes (NTs) and nanowires (NWs) were prepared by an alkaline hydrothermal synthesis procedure. The structural properties of the synthesized TiO<sub>2</sub> nanomaterials were investigated with high-resolution scanning electron microscopy (HR-SEM), transmission electron microscopy (TEM), high-resolution transmission electron microscopy (HR-TEM), atomic force microscopy (AFM), powder X-ray diffraction (XRD) and X-ray photoelectron spectroscopy (XPS). The NWs and NTs were characterized using Raman and Fourier transform infrared (FT-IR) spectroscopy as well as Brunauer–Emmett–Teller (BET) measurements. Surface properties, i.e.  $\text{pH}_{\text{iep}}$  and  $\text{pH}_{\text{pzc}}$  of NWs and NTs were determined from electrokinetic measurements, potentiometric mass and electrolyte titrations. The relative acidity for the NWs is found to be in the interval  $3 < \text{pH}_{\text{iep}} < 4$  in comparison with the NTs, with  $4 < \text{pH}_{\text{iep}} < 6$ . The observed differences in the relative acidity are correlated with differences in crystal structure of the studied nanomaterials and their resulting morphology. In addition, our results reveal a strong electrolyte effect on the characteristic points,  $\text{pH}_{\text{iep}}$  and  $\text{pH}_{\text{pzc}}$ , especially the higher cation affinity for both TiO<sub>2</sub> nanomaterials surfaces that has a significant effect on the pH of the system. Application of the multisite complexation (MUSIC) model yields a satisfactory description of the electrokinetic data and can explain observed salt effect.



## 1. INTRODUCTION

Low cost, high thermal and photochemical<sup>1</sup> stability have spurred the use of TiO<sub>2</sub> in applications as diverse as sensors, solid oxide fuel cells,<sup>2</sup> water purification<sup>3</sup> adsorption of radioactive metal ions and photocatalysis.<sup>4</sup> Lately, there is an increased interest for the one-dimensional TiO<sub>2</sub> nanomaterials, nanowires (NWs) and nanotubes (NTs), which are nanomaterials with superior properties compared to macroscopic TiO<sub>2</sub>.<sup>5,6</sup> In this context, most of the studies are oriented to the “bottom up” approach, i.e. new synthesis pathways which result in nanomaterials with improved physicochemical and structural properties, like crystal phase composition, morphology and specific surface area. Most of the ongoing studies are focused

on crystal structure determination as well as clarification of the formation mechanisms and conversion from one morphology to another.<sup>7,8</sup> Many nanomaterials are exposed to the aqueous solutions either because of their intended application, such as improving the quality of water and soil by degrading the organic pollutants, or as a waste. Exposure of the nanomaterials to aqueous solutions leads to changes in the surface charge of the nanomaterials in response to the pH, composition and the ionic strength of the solution. Therefore, for the successful

Received: December 11, 2014

Revised: July 31, 2015

application of the TiO<sub>2</sub> nanomaterials, besides the detailed physicochemical characterization the information about acid–base surface properties is required.

The general model used for describing the charging at metal oxide/aqueous electrolyte solution interface is the triple layer model (TLM) introduced by Davies et al.<sup>9</sup> (additional explanations can be found in ref 1. and in [Supporting Information Material](#)). The electrical interfacial layer (EIL) formed at the TiO<sub>2</sub> surface/aqueous solution electrolyte interface affects all the processes where the interface takes an active role such as colloid transport, adsorption of ions from the solution or catalysis.<sup>10</sup>

Unique physicochemical and structural properties that these TiO<sub>2</sub> nanomaterials exhibit is a consequence of their size, which can also interfere with their acid–base surface properties. Going down from the macroscopic to the nanoscopic domain might change the distribution, the geometry, as well as the coordination of atoms (Ti–O coordination) at the surface affecting the surface reactivity/acidity of the studied materials.<sup>11</sup> Several studies have shown that surface charge of the nanoparticles is correlated with their size, specific surface area and crystal phase and that it can be controlled by the pH and the ionic strength of the medium.<sup>12,13</sup> Grover et al.<sup>12</sup> investigated the effect of the crystal structure, surface area, surface charge, electrokinetic potential and metal loading on the photocatalytic performance of sodium NWs and NTs. Their results revealed that size and shape alter the surface charge and electrokinetic potential of the investigated samples, which in turn are strongly correlated with their photocatalytic performance. Suttiponparnit et al.<sup>13</sup> investigated the role of surface area, size and crystal phase of spherical TiO<sub>2</sub> nanomaterials with different sizes. Variation in the surface area and size significantly affects the electrokinetic potential. The effect of morphology and crystallinity on the surface reactivity of the nanosized anatase was also explored by Ahmad et al.<sup>14</sup> They have shown that surface reactivity of differently shaped nanosized anatase particles depends on the degree of the crystallinity and the presence of differently exposed surfaces. Kinisinger et al.<sup>15</sup> investigated combined effect of the pH and the crystal phase in a nanocrystalline titania on the surface properties with respect to photocatalysis of methylene blue. Past studies of the TiO<sub>2</sub> nanotubes, for example, yield isoelectric points (pH<sub>iep</sub>) ranging from 3.6 to 6.6 with the specific value dependent on the specific electrolyte used, its concentration, and the charge of the metal cation.<sup>16–19</sup> Although, less data is available for TiO<sub>2</sub> nanowires, isoelectric points (pH<sub>iep</sub>) ranging from 2.9 to 3.9 have been reported, and as found for the NTs, the values depend on the specific electrolyte used and its concentration in the electrokinetic measurements.<sup>20</sup> In fact, these results show a variation in the obtained pH<sub>iep</sub> utilizing the same electrolyte at the same concentration suggesting that there are other variables, as yet unidentified, that influence pH<sub>iep</sub>. However, literature search gives insufficient data about the effect of the ionic strength and pH on the NWs and NTs acid–base surface properties.<sup>12,16–19</sup> Most of the studies deal with surface properties of the TiO<sub>2</sub> nanoparticles, especially electrokinetic measurements and the effect of the ions on the pH<sub>iep</sub> shift. In this sense, detailed explanation of how TiO<sub>2</sub> one-dimensional nanomaterial's morphology, size and crystal phase influences acid–base surface properties is still lacking.

Charging of metal oxides nanomaterials can be elucidated through electrokinetic measurements<sup>21</sup> (electrokinetic potential), potentiometric mass<sup>22</sup> and acid–base<sup>23</sup> titrations

(determination of the surface charge density) as well as electrolyte titrations<sup>24</sup> for testing the effect of the ionic strength on various TiO<sub>2</sub> surfaces. The above-mentioned techniques enable determination of surface properties as well as effects of counterions (cations and anions) on metal oxide surfaces. Two characteristic points, the isoelectric point (pH<sub>iep</sub>) and point of zero charge (pH<sub>pzc</sub>) reveal metal oxide electroneutrality, pH<sub>eln</sub> as well as affinity of cations and anions for the metal oxide surface.<sup>25</sup> The isoelectric point (pH<sub>iep</sub>) refers to the point where the electrokinetic potential is zero according to the pH, while pH<sub>pzc</sub> describes the point where with no net surface charge due to the presence of the equal positively and negatively charged surface groups.

Acid–base properties of the polycrystalline TiO<sub>2</sub> surfaces, i.e. anatase, rutile and TiO<sub>2</sub> P25 are very well explored.<sup>22–27</sup> Besides common methods used for the pH<sub>iep</sub> and pH<sub>pzc</sub> determination, lately the atomic force microscopy<sup>28</sup> (AFM) and surface harmonic generation<sup>29</sup> (SHG) for the single crystals are used.

The experiments in this study aimed to explore and disclose the acid–base surface properties and the charging of the NWs and NTs surface in the aqueous solution as well as surface reactivity/acidity. Two distinct TiO<sub>2</sub> nanomaterials, NWs and NTs were prepared by the hydrothermal procedures developed by Kasuga et al.<sup>30</sup> The NWs and NTs are characterized in details to gain insights about their morphology, crystal phase and size which were further correlated with the obtained pH<sub>iep</sub> for the NWs and NTs. Results presented here highlight surface charging properties of the two different morphologies, NWs and NTs, and the effect of a common electrolyte, NaNO<sub>3</sub>, on the characteristic points, isoelectric point and point of zero charge, intrinsic parameters that are first step in the quantification of the effect of the morphology, crystal phase and size on the surface reactivity/acidity. The MUSIC model was applied as attempt to quantify the differences observed in the acid–base surface properties as well as the salt effect on the NWs and NTs.

## 2. EXPERIMENTAL SECTION

**2.1. Synthesis of the TiO<sub>2</sub> nanomaterials.** NWs and NTs powders were prepared by alkaline hydrothermal procedure by suspending 2.0 g of TiO<sub>2</sub> P25 (75% Anatase, 25% Rutile Degussa) with aqueous 65 cm<sup>3</sup> NaOH solution (*c* = 10 mol dm<sup>-3</sup>). The preparation procedure for NTs and NWs differs. Preparation of NTs requires a lower temperature and longer duration time of the synthesis (*θ* = 146 °C, *t* = 48 h) as opposed to nanowires where is vice versa (*θ* = 190 °C, *t* = 24 h). Suspensions were stirred with a magnetic stirrer and repetitively sonicated (1500 V, 20 kHz, Sonicator Ultrasonic Processor XL, Misonix Inc.) for 5 min followed by 5 min off for a total of 2 h. Prepared suspensions were transferred into the Teflon lined autoclave. The resulting precipitates were filtered and extensively washed with deionized water, (due to the presence of NaOH impurities that remained after synthesis) until the conductivity and pH were close to values for deionized water (pH ≈ 6.5, *κ* < 10 μS cm<sup>-1</sup>). The sample was stirred in 0.1 M HCl for 3 h to remove excess of adsorbed Na<sup>+</sup> ions. The resulting product was again filtered and washed extensively with deionized water to remove acidic impurities until the conductivity and pH of the supernatant was below 10 μS cm<sup>-1</sup> and at pH ≈ 6.5. The NWs and NTs were dried at 80 °C for 6 h in air and stored in glass bottles.

## 2.2. Characterization of the TiO<sub>2</sub> nanomaterials.

Morphology of NWs and NTs was studied by high-resolution scanning electron microscopy (HR-SEM), transmission electron microscopy (TEM), high-resolution transmission electron microscopy (HR-TEM), atomic force microscopy (AFM) and powder X-ray diffraction (XRD).

Morphological studies on NWs and NTs have been performed using high-resolution scanning electron microscopy (HR-SEM) on a Zeiss HR-SEM (Gemini Class) at 3–5 kV to check for continuity, shape, length and morphology of different TiO<sub>2</sub> samples.

Transmission electron microscopy (TEM) and high-resolution TEM (HR-TEM) of the samples were performed using a Philips FEG CM200 transmission electron microscope operated at 200 kV. For the TEM analysis samples of nanotubes and nanowires were first suspended in chloroform by sonication; then, a small drop of the suspension was transferred onto the carbon-coated copper grid. Finally, the grid was dried in air.

For the AFM measurements samples were prepared as follows. Suspensions of the NWs or NTs were prepared by sonication using a bath sonicator (35 kHz, 320 W, Bandelin Sonorex Rk 100 H) for 10 min before AFM measurements. A droplet of suspension of NWs or NTs in deionized water ( $\gamma = 1 \text{ g dm}^{-3}$ , volume of the droplet was 15  $\mu\text{L}$ ) was deposited on a freshly cleaved mica sheet. Another piece of freshly cleaved mica was put on top and the solution was smeared across the sample to ensure the spread of NWs or NTs without formation of big agglomerates. Samples were then left to dry for approximately 10 min before the imaging. The AFM imaging was performed with a Nanosurf FlexAFM in dynamic force mode (simultaneously acquiring topography, amplitude and phase images) under ambient conditions. AFM probes were obtained from AppNano (ACLA silicon tips of nominal spring constant 20–95  $\text{N m}^{-1}$  with tip radius less than 10 nm and nominal resonant frequency of 145–230 kHz). During the measurement vibration frequency was 189 kHz with vibration amplitude of 150 mV. For both samples, imaging was performed on several different places on the sample, and features observed for the each sample were consistent between the different spots on the same sample. Subsequently, AFM images were processed by Gwyddion software.<sup>31</sup>

Powder X-ray diffraction was applied by using a PHILIPS PW 1840 at 40 kV and 40 mA with Cu K $\alpha$  radiation ( $\lambda = 0.154056 \text{ nm}$ ). The XRD data were analyzed using the Philips X'Pert Graphics & Identify software package.<sup>32</sup>

X-ray photoelectron spectroscopy (XPS) measurements were performed with a XPS-Analyzer. For sample preparation a small amount of dry powder was tipped on a carbon strip mounted on a standard sample holder by Prevac and pressed to a solid layer. After load-locking to the ultrahigh vacuum system the powders were pumped out over several hours in a pressure range about  $10^{-7}$  mbar and heated from time to time by a chamber-installed halide lamp. Photoelectronic measurements were performed with generated X-rays from an aluminum K $\alpha$  anode under  $10^{-9}$  mbar vacuum conditions. The pass energy of the XPS-Analyzer was set to 200 eV. Results obtained from the XPS measurements are given in the Supporting Information Material.

Raman scattering measurements were carried out on a EQUINOX 55 device using the Nd:YAG laser ( $\lambda = 1064 \text{ nm}$ ) at room temperature. The Raman spectra were recorded by

applying a laser power of 100 mW. The measurement step of the Raman spectrophotometer was  $4 \text{ cm}^{-1}$ .

Fourier transform infrared spectroscopy measurements were carried out on a PerkinElmer FT-IR C89391 device at the room temperature. The step of the FT-IR spectrophotometer was  $2 \text{ cm}^{-1}$ . Results obtained from the Raman and FT-IR spectroscopy are given in the Supporting Information Material.

The specific surface area,  $s$ , was determined employing the multipoint Brunauer–Emmett–Teller method using N<sub>2</sub> as adsorbed gas at 77 K and relative pressure values in the range 0.05–0.3 on a Micrometrics Instrument Corporation, Gemini V series Surface Area Analyzer.

## 2.3. Surface properties of TiO<sub>2</sub> nanomaterials.

**2.3.1. Determination of the electrokinetic potential.** Electrokinetic potential measurements of NWs and NTs were probed via ZetaPlus, Zeta potential Analyzer, Brookhaven 90Plus/BIMAS. For electrokinetic measurements  $0.025 \text{ g dm}^{-3}$  NWs or NTs suspensions were prepared in the NaNO<sub>3</sub> aqueous solution at two ionic strengths:  $I_c = 1 \text{ mM}$  and  $I_c = 10 \text{ mM}$ . Initial pH,  $\text{pH}_0 \approx 10$  of the NWs or NTs suspensions was adjusted with 0.1 M NaOH. Suspensions were sonicated for the 5 min using the bath sonicator (35 kHz, 90–160 W, ultrasonic energy density was in the range  $27\text{--}48 \text{ kJ dm}^{-3}$ , Bandelin Sonorex Rk 100 H) before electrokinetic measurements. After each addition of the titrant (0.1 M HNO<sub>3</sub>), the suspension was left to equilibrate for 5 min. That time was required to obtain stable pH electrode signal response with the potentiometer accuracy of 0.01 mV. In order to prevent sedimentation, stirring was applied during the measurement.

All experiments were carried and under nitrogen atmosphere at 25 °C. Data was collected with ten runs per measurement for two measurements total. Reproducibility of the electrokinetic measurements is presented in the Supporting Information Material.

**2.3.2. Potentiometric mass titration.** Potentiometric mass titrations were performed to determine the effect of ionic strength on the point of zero charge for NWs and NTs samples as a function of pH. In comparison to potentiometric acid–base titrations, potentiometric mass titration is a method of choice in the case of the nonsymmetrical electrolyte adsorption but is valid only in the case when the sample is free from the impurities (acidic or basic impurities that remained from synthesis procedure).<sup>33</sup> Besides that, another advantage of performing the experiments at low ionic strength is that it is not necessary to perform blank titration to determine surface charge like for potentiometric acid–base titrations. The potentiometric mass titration can be performed by subsequent addition of the powder to the pure water or aqueous electrolyte solution at certain pH and the ionic strength and measuring the pH of the suspension. The pH of the suspension changes gradually and approaches a constant value,  $\text{pH}_\infty$  at high mass concentration. The final pH,  $\text{pH}_\infty$  corresponds to the point of zero charge ( $\text{pH}_{\text{pzc}}$ ) in the samples that are extensively washed during the synthesis procedure so that all acidic and basic impurities are removed. From the mass titration data surface charge<sup>34</sup> can be calculated using the following equation

$$\sigma_0 = -\frac{F}{s\gamma}(10^{-\text{pH}_\gamma} - 10^{-\text{pH}_0} - 10^{\text{pH}_\gamma - \text{p}K_{\text{w},c}^\circ} + 10^{\text{pH}_0 - \text{p}K_{\text{w},c}^\circ}) \quad (3)$$

where  $\sigma_0$  denotes the surface charge,  $F$  is Faraday's constant,  $s$  is specific surface area,  $\gamma$  is mass concentration,  $\text{pH}_\gamma$  is pH at the certain mass concentration  $\gamma$ ,  $\text{pH}_0$  is pH of aqueous electrolyte

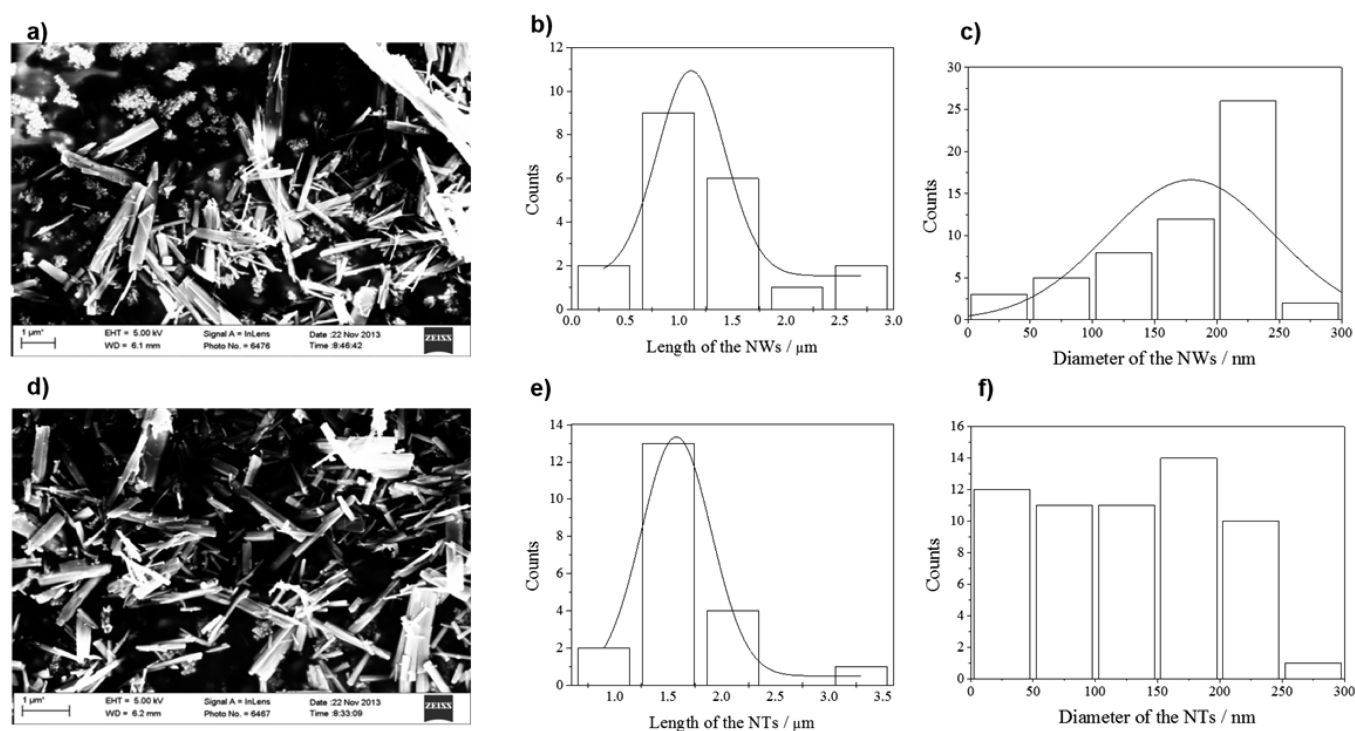


**Figure 1.** HR-SEM micrographs and the size profiles of the prepared  $\text{TiO}_2$  nanomaterials by the hydrothermal synthesis route. a), b), c) NWs, d), e), f) NTs.

solution without added particles and  $K_{w,c}^\circ$  is thermodynamic dissociation constant for water,<sup>35</sup>  $\text{p}K_{w,c}^\circ = -\log(K_{w,c}^\circ) = 14$  at 25 °C.

In the  $\text{NaNO}_3$  aqueous electrolyte solution at  $\text{pH}_0 \approx 7$  and ionic strength of  $I_{c,0} = 0.1$  mM and  $I_{c,0} = 10$  mM, precise amounts of the NWs and NTs solid powder were added sequentially. After each addition, the suspension was stirred with a magnetic stirrer for 1 min, sonicated for 2 min, stirred for five additional minutes and then the pH was recorded until it reached a constant value,  $\text{pH}_\infty$ . At this point, further additions of powder did not produce a significant pH change. From the mass titration, the point of zero charge is taken to be  $\text{pH}_\infty = \text{pH}_{\text{pzc}}$  due to the fact that the acidic and basic impurities were removed by extensive washing. All measurements were carried out under nitrogen atmosphere at 25 °C.

**2.3.3. Potentiometric electrolyte titration.** The effect of the ionic strength on the NWs and NTs samples as a function of pH was investigated with potentiometric electrolyte titration. Starting with NWs or NTs at high mass concentration to make sure that  $\text{pH}_\infty$  was reached, dense suspensions of NWs or NTs were prepared by the addition of a large amount of NWs or NTs powder to aqueous  $\text{NaNO}_3$  at initial ionic strength,  $I_{c,0} = 0.1$  mM. To minimize changes in ionic strength due to the addition of  $\text{NaNO}_3$  solution, small volumes of concentrated  $\text{NaNO}_3$  solution (corresponding to <5% of the total solution volume) were added. To achieve higher ionic strengths, weighed portions of solid  $\text{NaNO}_3$  were added to the NWs and NTs solutions. After each addition, the suspensions were stirred with magnetic stirrer for 1 min, and then sonicated for 2 min. The suspension was then stirred for 5 min and the pH was measured. The procedure was repeated until ionic strength increased from 0.1 mM to 0.1 M.

**2.4. Surface complexation modeling.** The charging behavior and surface protonation constants for the NWs and NTs were determined by the means of multisite complexation

(MUSIC) model.<sup>36</sup> The MUSIC model framework combines the macroscopic experimental data with surface structural properties on the molecular level.<sup>37</sup> Within the MUSIC model, charging behavior of the metal oxides and the various types of the surface groups are correlated on the basis of the geometric data of the acid–base surface sites. The MUSIC model gives good estimation for the intrinsic protonation constant,  $\log K_p$  for a given surface.

### 3. RESULTS AND DISCUSSION

**3.1. Synthesis and characterization of the  $\text{TiO}_2$  nanomaterials.** Two distinct  $\text{TiO}_2$  morphologies, NWs and NTs were synthesized using the hydrothermal route. Figure 1 shows high-resolution scanning electron microscopy micrographs (Figure 1 a) and d)), length distributions (Figure 1 b) and e)) and the diameter (Figure 1 c) and f)) of the NWs and NTs samples.

HR-SEM analyses of the  $\text{TiO}_2$  samples (Figure 1) have shown that the diameters of NWs are in the range of  $\approx 50$ –300 nm, the same as the diameters of the NTs. In general, the length of the NWs (500–3000 nm), was shorter than that found for the NTs (1000–3500 nm). Purely based just on the surface analysis of the sample, with the HR-SEM it was not possible to observe the difference between NWs and NTs, due to their agglomeration.

TEM and HR-TEM measurements were performed to confirm the NWs and NTs morphology in the prepared samples. Figures 2 a) and b) show TEM images of NWs. The obtained NWs crystallized in  $\text{TiO}_2$ -B phase in monoclinic structure with lattice parameters  $a = 1.217$  nm,  $b = 0.374$  nm,  $c = 0.652$  nm;  $\beta = 107.054^\circ$  which was confirmed by the selected area diffraction (SAED, inset in Figure 2b)). Figure 2 c) shows high resolution TEM images of  $\text{TiO}_2$ -B NWs in which lattice fringes distance of 0.37 and 0.65 nm corresponds to (110) and

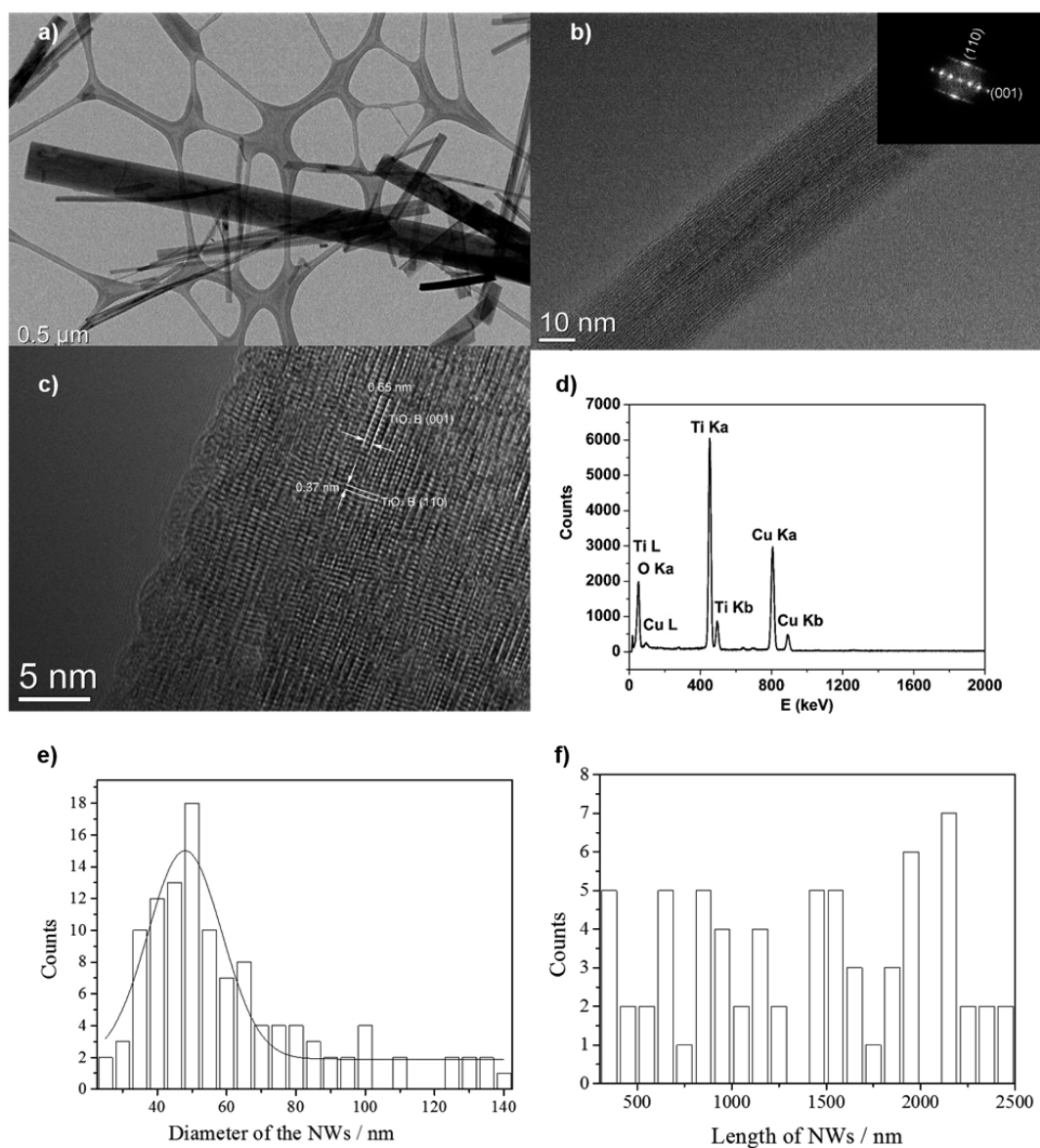


**Figure 2.** TEM analysis of the NWs. a) TEM of the NWs, b) HR-TEM of the NWs (the inset in Figure 2 b)) with diffuse Fast Fourier Transform, FFT rings, correspond to FFT pattern of TiO<sub>2</sub>-B NWs; c) HR-TEM image of NWs in which grows in (110) direction, d) EDXS spectra of the NWs; e) histograms of diameter distribution of the NWs; f) histograms of length distribution of the NWs.

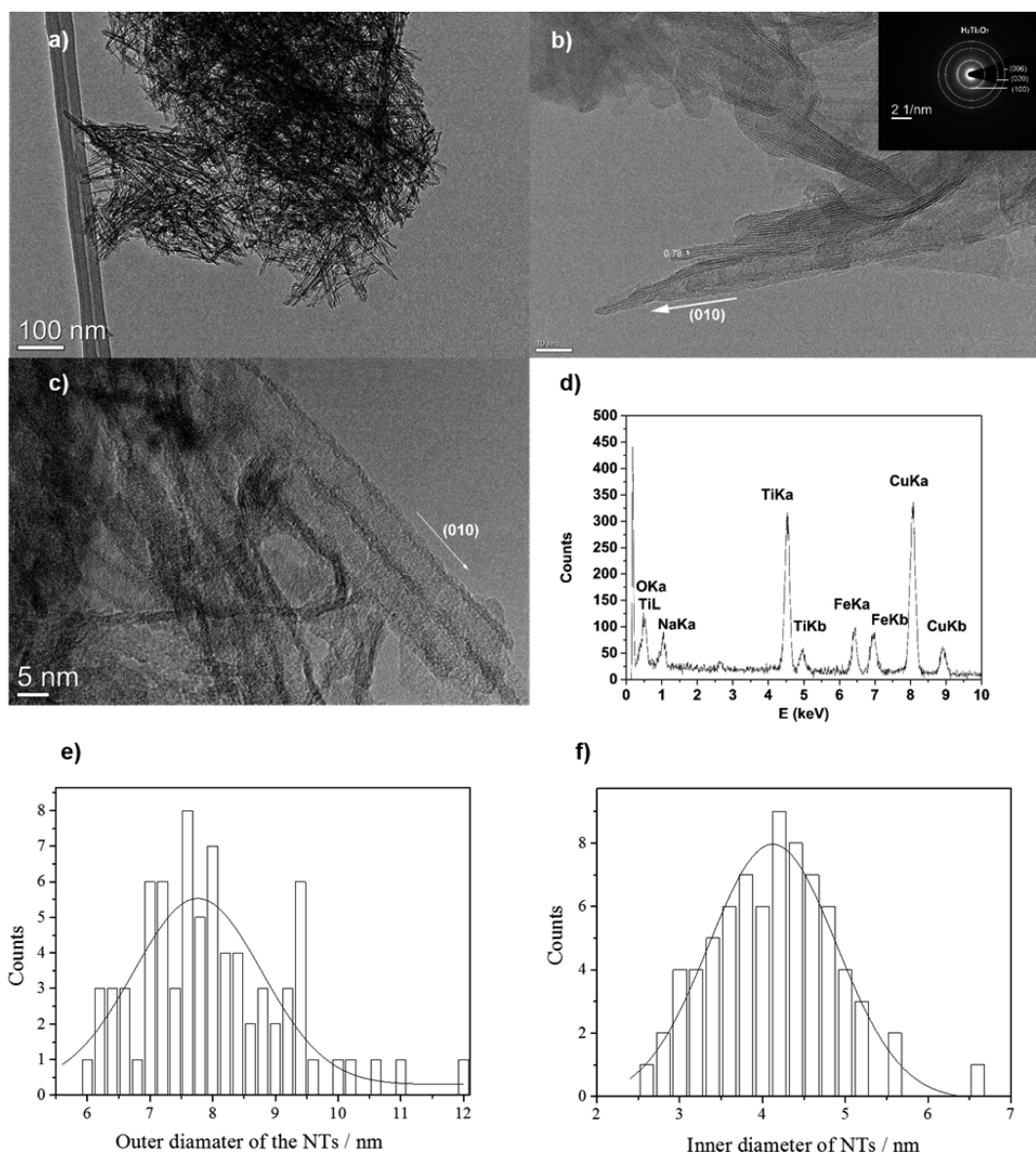
(001) planes of TiO<sub>2</sub>-B phase. The Energy Dispersive X-ray Spectroscopy (EDXS) analysis (Figure 2 d)) confirms the presence of only oxygen and titanium atoms in the crystal structure. For the NWs the diameter and length distribution are shown on Figure 2 e) and f). The obtained results show a quite broad distribution of diameter and length for the NWs. The average diameter of NWs is 48 nm, and the average length was not possible to calculate due to too wide size distribution from less than 500 nm up to 2500 nm.

Figure 3 a) and b) shows TEM images of the NTs nanostructure with tubular morphology. The NTs exhibit multilayer formation with an interlayer distance of 0.78 nm. The formation of protonated type of H<sub>2</sub>Ti<sub>3</sub>O<sub>7</sub> NTs with monoclinic structure was confirmed by selected area diffraction (SAED, inset in Figure 3 b)) while EDXS, showed no presence of Na atoms.

This indicates that their exchange with H<sup>+</sup> ions after hydrothermal synthesis was complete. From TEM and HR-TEM inner and outer diameter size distribution of NTs was

determined. The NTs have average inner diameter of 4.12 nm and the outer diameter is 7.8 nm. The length distribution was not possible to measure due to, too strong agglomeration of NTs. Calculated inner and outer diameter size distributions from TEM images are shown on Figure 3 e) and f). Also was not possible to calculate the aspect ratio of synthesized NWs and NTs because of unknown values for the average length of NWs and NTs.

A typical AFM picture of one area of a NWs sample is shown in Figure 4. Distinct straight wire-like shapes-NWs, are clearly visible, with tendency to form bunches from a pair or more NWs sticking together (more or less in parallel). However, single NWs are also quite frequent. There is no observable preference in direction among different bunches and single NWs and they are all oriented in random directions. Some polydispersity in both lengths and diameters of the NWs is observed from AFM topographs with radius of a single NW varying between 50–200 nm, while lengths vary from rather



**Figure 3.** TEM analysis of the NTs. a) TEM of the NTs, b) HR-TEM of the NTs (the inset in Figure 3 b) with diffuse Fast Fourier Transform, FFT rings, correspond to FFT pattern of protonated NTs ( $\text{H}_2\text{Ti}_3\text{O}_7$ ); c) HR-TEM image of NTs in which grows in (010) direction, d) EDXS spectra of the NTs; e) histograms of outer diameter distribution of the NTs; f) histograms of inner diameter distribution of the NTs.

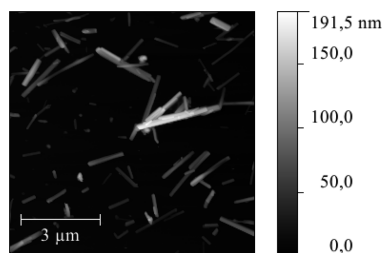


**Figure 4.** Typical topography image of the NWs deposited onto mica surface. Higher areas are depicted with the lighter color, according to the scale bar on the right.

short fragments of a few hundred nm (around 200 nm) to several microns (cca 3  $\mu\text{m}$ ).

In the sample with deposited NTs only small clusters (with size varying from below 100 nm to 1  $\mu\text{m}$ ) with no discernible features resembling NTs were observed (not shown). It is

assumed that they either broke during the preparation and that the fragments agglomerated or that they are too small for their distinct features to be observed via this method.

On Figure 5 the powder XRD patterns of the NWs and NTs are shown as well as the ones of the initial  $\text{TiO}_2$  sample used for the synthesis ( $\text{TiO}_2$  P25), anatase, rutile and  $\text{TiO}_2$ -B phase. The powder XRD pattern of NWs reveals presence of the mixed phases, layered titanates and  $\text{TiO}_2$ -B. The diffraction peaks at the  $2\theta$  position of  $8.0^\circ$  and  $11.0^\circ$  correspond to (001) and (200) reflections, respectively, and are characteristic for layered titanates (H). Similar patterns were obtained in the work of Darányi et al.,<sup>38</sup> Suzuki et al.<sup>39</sup> and in work of Bayykin and Walsh.<sup>40</sup> Additional peaks were at the  $24.9^\circ$  (110) and  $48.4^\circ$  (020). The obtained diffraction peaks are attributed to  $\text{TiO}_2$ -B phase (JCPDS 74-1940).<sup>41,42</sup> The  $2\theta$  values of  $\text{TiO}_2$ -B peaks are similar to those of anatase but much broader which is mainly due to the dimensional confinement. According to the TEM and HR-TEM results (Figure 2a) and b) as well

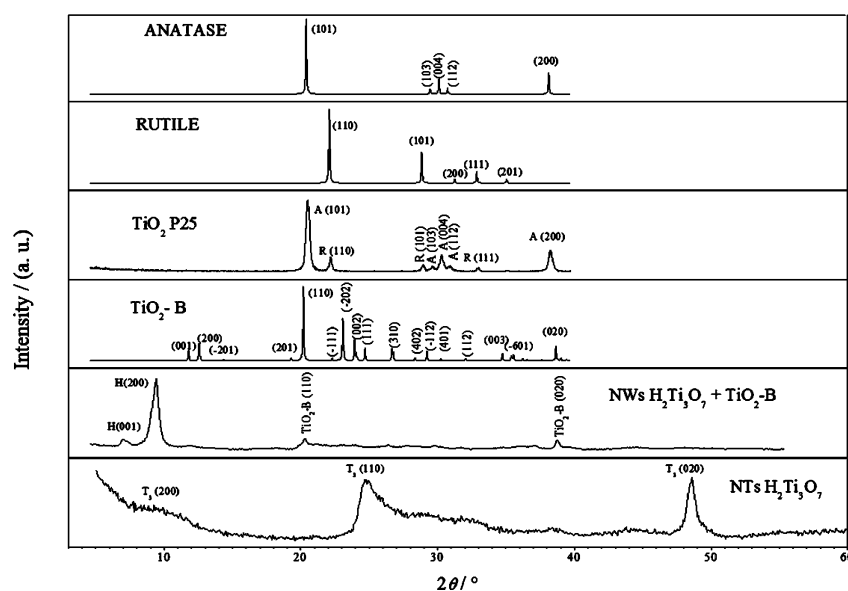


**Figure 5.** Powder X-ray diffraction patterns of the TiO<sub>2</sub> nanomaterials. Pure anatase, rutile and TiO<sub>2</sub>-B crystal forms provided from the Inorganic Crystal Structure Database, initial material used in the synthesis (TiO<sub>2</sub> P25) and obtained powders, NWs and NTs. A: anatase (JCPDS 78–24586), R: rutile (JCPDS 87–0710), T3: H<sub>2</sub>Ti<sub>3</sub>O<sub>7</sub> (JCPDS 36–0654), TiO<sub>2</sub>-B (JCPDS 74–1940), H: NWs-layered titanates.

as the Raman and FT-IR measurements (Supporting Information Material, Figure S5 and S6) the NWs sample is assigned as the TiO<sub>2</sub>-B phase. Bavykin and Walsh<sup>43</sup> pointed out that XRD as a method for the characterization of the NWs and NTs should be taken attentively. The obtained discrepancy between XRD and HR-TEM, Raman and FT-IR can be explained in terms of the different crystal modifications of the TiO<sub>2</sub> (anatase, rutile and brookite) and the polytitanic acids.

Peak broadening in XRD patterns of the NWs and NTs was observed. This can be caused by the small nanocrystals size. In addition, during the formation of the NWs and NTs, wrapping along a certain crystallographic axis could lead to the broadening of the peaks which makes the interpretation of the Miller index more difficult. Furthermore, the NWs and NTs can undergo the phase transformation during and after the synthesis due to their instability.

XRD data for the NTs correspond to the typical XRD pattern of protonated titanate (H<sub>2</sub>Ti<sub>3</sub>O<sub>7</sub>) NTs.<sup>44</sup> In addition, several characteristic diffraction peaks of NTs, which correspond to crystalline planes T3 (200), T3 (110) and T3 (020) (JCPDS 36–0654) T3-monoclinic (H<sub>2</sub>Ti<sub>3</sub>O<sub>7</sub>) were observed.

Details of NWs and NTs XPS studies are given in Supporting Information Material. NWs and NTs spectra contained Ti 2p<sub>3/2</sub> and Ti 2p<sub>1/2</sub> peaks, with a binding energy of 459 and 465 eV (Figure S3). The binding energy of the 459 eV (Ti 2p<sub>3/2</sub>) can be attributed to Ti<sup>4+</sup> in TiO<sub>2</sub>. The measured O 1s peak (Figure S4) with binding energy located at 531 eV can be attributed to physically and crystallographic adsorbed water. Data obtained from the XPS analysis are in a good agreement with the data reported in literature.<sup>45–49</sup>

Raman and FT-IR spectra of the prepared TiO<sub>2</sub> nanostructures show spectral differences between the two structures (obtained spectra are presented in the Supporting Information Material). The absorption bands observed in the Raman spectra (148, 192, 269, 292, 345, 372, 432, 452, 599, and 673 cm<sup>-1</sup>) and in the FT-IR spectra (3400–2942, 1630, 930 and 700–450 cm<sup>-1</sup>) of the NWs are in good agreement with previously published results for Raman spectra of TiO<sub>2</sub> (B) nano-

wires.<sup>41,42,50,51</sup> Raman spectra (bands at 152, 189, 268, 386, 450, and 657 cm<sup>-1</sup>) and FT-IR spectra (bands at 3370–2843, 1632, 930 and 793–411 and 491 cm<sup>-1</sup>) of the NTs confirmed the close resemblance between the obtained spectra and those published previously.<sup>44,52</sup>

As expected, the major difference is in the specific surface area, *s* of the two samples. Nitrogen adsorption isotherms (BET), yield 314.5 m<sup>2</sup> g<sup>-1</sup> for the specific surface area of the NTs, and for the NWs specific surface area of 28.5 m<sup>2</sup> g<sup>-1</sup> has been determined. The difference in the specific surface area is a consequence of NTs multilayered hollow structure as opposed to NWs.

**3.2. Surface properties of TiO<sub>2</sub> nanomaterials.** Surface ≡TiOH groups play an important role in surface reaction mechanism in the various processes that take part at the TiO<sub>2</sub> surface/aqueous electrolyte solution interface. Besides adsorption of the reactant molecules, ≡TiOH surface groups also take part in trapping the photogenerated holes by forming hydroxyl radicals.<sup>53–55</sup>

The active surface groups (≡TiOH) at the TiO<sub>2</sub> surface are amphoteric and they can take up or release protons. Surface complex formation equilibria is characterized in terms of the adsorption of the H<sup>+</sup>, OH<sup>-</sup>, cations and ligands at the metal oxide surface. According to Stumm et al.<sup>56</sup> definition of surface charge as interaction of the active surface groups with the H<sup>+</sup> and the OH<sup>-</sup> ions pH<sub>pzc</sub> does not characterize a point of effective zero charge. Binding of the cations increase the effective charge of the surface, leading to the observed shifts in the pH<sub>iep</sub> and pH<sub>pzc</sub> as the ionic strength increases. Sposito<sup>57</sup> pointed out that the pH<sub>pzc</sub> refers to the pH value where the total net particle charge is zero, including any contributions from cations or anions besides those from H<sup>+</sup> or OH<sup>-</sup> adsorbed in the electrical double layer. If there are negligible or equivalent affinities for cations and anions to the TiO<sub>2</sub> surface, there would be no change in pH<sub>iep</sub> or pH<sub>pzc</sub>. Surface complex formation is a competitive process between cations and H<sup>+</sup> ions. Binding of the cations on the metal oxide surface is strongly pH-dependent process. In the lower pH region, the positively surface charged sites dominate and repulsion forces

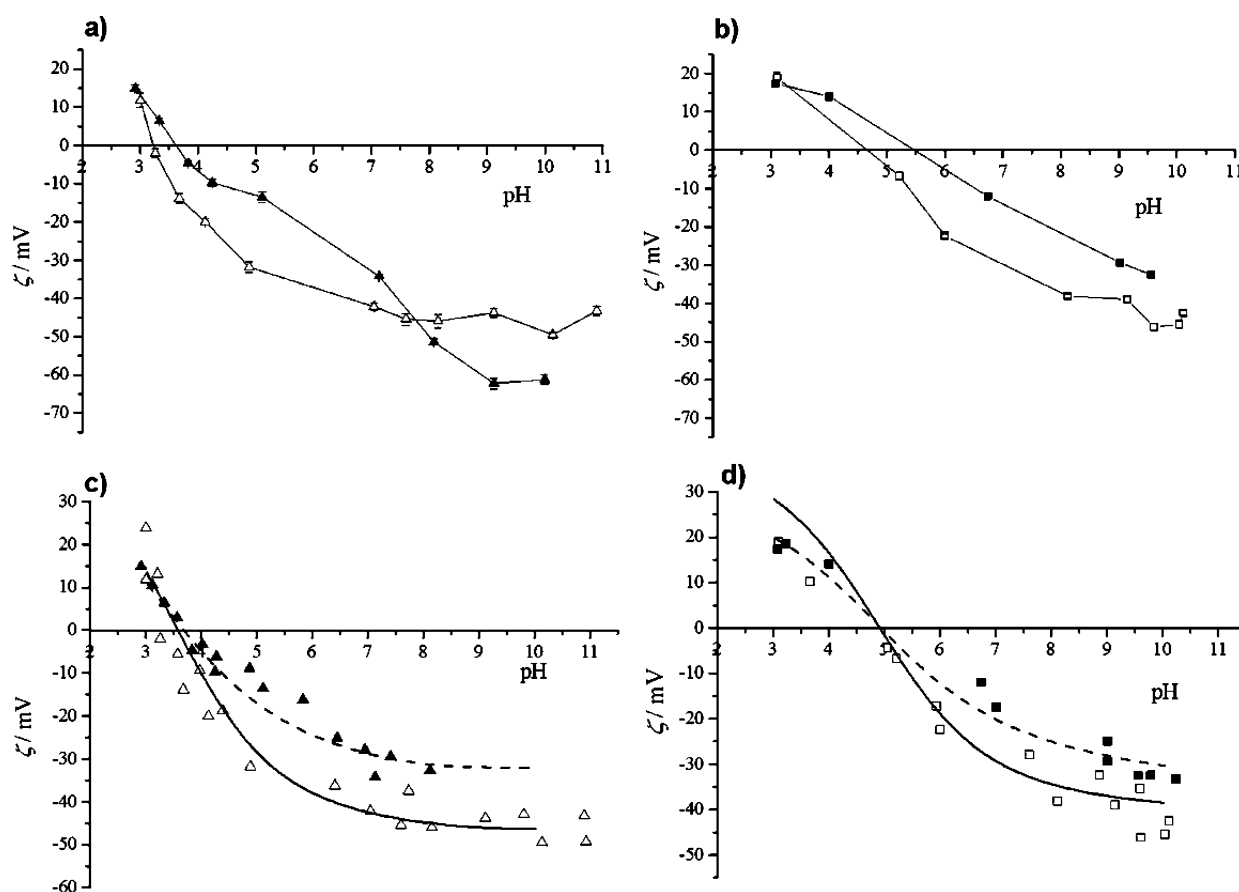


**Figure 6.** Experimental data: electrokinetic potential of  $\text{TiO}_2$  nanomaterials in  $\text{NaNO}_3$  aqueous electrolyte solution. a) NWs: ( $\Delta$ )  $I_c = 1$  mM, ( $\blacktriangle$ )  $I_c = 10$  mM; b) NTs: ( $\square$ )  $I_c = 1$  mM, ( $\blacksquare$ )  $I_c = 10$  mM.  $\gamma = 0.025$  g  $\text{dm}^{-3}$ ,  $\vartheta = 25$  °C. Modeling: results of the electrokinetic potential measurements of the (c) NWs and (d) NTs at different ionic strengths in  $\text{NaNO}_3$  aqueous electrolyte solution. Experimental results were fitted using the MUSIC model. Lines are model calculations using the parameters in Table 2. (—)  $I_c = 1$  mM, (---)  $I_c = 10$  mM.

between the surface and the cations are enhanced leading to the reduced cations binding. The electrokinetic potential of the NWs and NTs as a function of pH is represented in Figure 6 a) and b) which further reveals the isoelectric point for the NWs and NTs and their dependence on the ionic strength ( $I_c = 1$  mM and  $I_c = 10$  mM). The values for the  $\text{pH}_{\text{iep}}$  at two ionic strengths for both NWs and NTs are given in Table 1.

**Table 1.** Isoelectric point for NWs and NTs samples at two ionic strengths,  $I_c = 1$  mM and  $I_c = 10$  mM determined from electrokinetic measurements.  $\Delta\text{pH}_{\text{iep}} = \text{pH}_{\text{iep}}(I_c = 10 \text{ mM}) - \text{pH}_{\text{iep}}(I_c = 1 \text{ mM})$

$\text{TiO}_2$ nanomaterial	$\text{pH}_{\text{iep}}$		$\Delta\text{pH}_{\text{iep}}$
	$I_c = 1$ mM	$I_c = 10$ mM	
NWs	3.2	3.6	0.4
NTs	4.6	5.5	0.9

Obviously, the crystal phase and the morphology of NWs and NTs affect their surface properties. NTs are hollow tubular nanomaterials with internal multilayered walls with the number of layers varying between 2 and 10.<sup>58</sup> NWs are solid, longer than NTs and without internal layered structure. NTs structures consisting of cylinders with hollow cavity and multilayered walls result in increased specific surface area as well as porosity, compared to the NWs. Larger surface area of

the NTs, due to their layered structure, could be the reason for the significant shift of their  $\text{pH}_{\text{iep}}$  compared to NWs.

Electrokinetic potential and shift in the  $\text{pH}_{\text{iep}}$  of the NWs and NTs are strongly correlated with the crystal planes exposed to the aqueous electrolyte solution, the density of active surface sites where protonation and deprotonation occur as well as the adsorption of the counterions.<sup>10,59,60</sup> Domination of the present crystal planes are reflected in the type and number of surface sites. Crystal planes of a given material could have different coordination of the oxygen atoms—singly, doubly or triply coordinated, which differs in bond length and the position at the surface, thus affecting the proton affinity. Unequal affinity of the counterions is attributed to the specific adsorption of the cations or the anions, thus affecting the cation or anion adsorption thermodynamic equilibrium constant, leading to the shift of the  $\text{pH}_{\text{iep}}$  as the ionic strength increase.<sup>10</sup> In addition, the isoelectric point of NWs is in a more acidic region,  $\text{pH} = 3\text{--}4$ , compared to NTs, which isoelectric point is in the  $\text{pH} = 4\text{--}6$  region. There are two main reasons for different  $\text{pH}_{\text{iep}}$  of the nanomaterials according to Borghi et al.<sup>61</sup> Morphology of nanomaterials might change the local chemical environment, i.e. active surface groups, their availability on the surface as well as electrical interfacial layer. The other possible explanation is that there is more than one type of surface groups on the NTs surface so the  $\text{pH}_{\text{iep}}$  is higher than the one of NWs.

Different affinities of ions for the  $\text{TiO}_2$  surface influence the surface properties of the investigated samples. In our study, all

experiments were performed in  $\text{NaNO}_3$  aqueous electrolyte solution so the effect of the type of the electrolyte is excluded. The surface of the NTs corresponds to the (100) plane which is abundant with  $-\text{OH}$  groups,<sup>43</sup> leading to the decrease in the surface acidity and shift to the higher pH than NWs. Correlation of the crystal structure of the NWs and NTs with the obtained isoelectric point leads to the conclusion that different crystal faces exposed on the surface cause the surface heterogeneity and surface reactivity/acidity. Acid–base behavior of NWs and NTs is a superposition of the contributions from the reaction sites of the different crystal planes. Ahmad et al.<sup>14</sup> emphasized the complex correlation of the acid–base surface properties with surface acidity and surface heterogeneity as well as crystallinity, surface area and crystal plane properties. To understand acid–base equilibria of the NWs and NTs we should take into account exposed crystal planes and their effects on the surface reactivity/acidity. The samples prepared for this study are nanocrystals and their XRD exhibit lower intensity and broader peaks in comparison to starting material ( $\text{TiO}_2$  P25) used for the synthesis. Besides that, crystal planes on the NWs and NTs surface are convex, which makes the correlation of the surface reactivity/acidity with the observed isoelectric point more complex than in the case of the flat crystal planes e.g. in  $\text{TiO}_2$  polished single crystal samples. For the detailed analysis of the displayed crystal planes based on the TEM images and XRD patterns and their correlation with the observed isoelectric points in both samples the MUSIC model<sup>40</sup> is applied. MUSIC model enables determination of the surface protonation constants for the NWs and the NTs. The proton affinity of different surface groups of the NWs and NTs were calculated applying an approach based on work by Machesky et al.<sup>37</sup> involving  $R_0 = 1.803 \text{ \AA}$  and  $b = 0.37$ . These values were used by the cited authors for rutile to calculate bond valences within the revised multisite complexation (MUSIC) model and involving a basic Stern electrostatic model. We attempted to model the macroscopic data, i.e. electrokinetic potentials. We started from the available structures of the two polymorphs using structure data from Gateshki et al.<sup>62</sup> for the NWs and from Feist and Davies for the NTs.<sup>63</sup> The structure was inspected for potential functional groups that might be relevant for the observed isoelectric points. For the NWs the structural data yield a singly coordinated oxygen with a Ti–O distance of  $1.87 \text{ \AA}$  as a candidate that appears reasonable for describing the experimental observations for the electrokinetic potentials. This would yield an intrinsic protonation constant,  $\log K_p$ , for protonation of the group of 3.74. Since precise determination of all groups and their concomitant properties was not possible from the obtained XRD data, we use this value with a 1-pK formalism and fractional charges of  $+(1/2)$  and  $-(1/2)$ . The model requires furthermore the interfacial capacitance and electrolyte binding constants as well as a site density. The latter was fixed at 8 sites/ $\text{nm}^2$ . The precise value of the site density cannot be determined from the available data, but is not a crucial parameter either for this kind of modeling. On the plane where the singly coordinated group occurs, no other groups appear, so that we choose a relatively high site density. We also stress that the aim of the modeling exercise is to verify if the structure of the polymorphs can explain the observed isoelectric points ( $\text{pH}_{\text{iep}}$ ). In the case of the NTs a singly coordinated oxygen occurs with a Ti–O distance of  $1.884 \text{ \AA}$ . This would yield an intrinsic protonation constant,  $\log K_p$ , for protonation of the group of 4.67. With a site density of  $2.1 \text{ sites}/\text{nm}^2$ , which

is in the range often found in literature,<sup>64</sup> the parameters given in Table 2 are finally obtained and a reasonable description of

**Table 2. Surface complexation parameters for a tentative description of the electrokinetic data**

SAMPLE	REACTION EQUATION	$\log K$	C/F $\text{m}^{-2}$	slip plane parameter/nm
NWs	$\equiv\text{TiOH}^{-1/2} + \text{H}^+ \rightleftharpoons \equiv\text{TiOH}_2^{+1/2}$	3.74	0.70	0.70
	$\equiv\text{TiOH}^{-1/2} + \text{Na}^+ \rightleftharpoons \equiv\text{TiOH}^{-1/2} \cdot \text{Na}^+$	−0.20		
	$\equiv\text{TiOH}^{+1/2} + \text{NO}_3^- \rightleftharpoons \equiv\text{TiOH}^{+1/2} \cdot \text{NO}_3^-$	−0.64		
	$\equiv\text{TiOH}^{-1/2} + \text{H}^+ \rightleftharpoons \equiv\text{TiOH}_2^{+1/2}$	4.67	0.34	0.89
NTs	$\equiv\text{TiOH}^{-1/2} + \text{Na}^+ \rightleftharpoons \equiv\text{TiOH}^{-1/2} \cdot \text{Na}^+$	−0.30		
	$\equiv\text{TiOH}^{+1/2} + \text{NO}_3^- \rightleftharpoons \equiv\text{TiOH}^{+1/2} \cdot \text{NO}_3^-$	−0.84		

the electrokinetic potentials is possible as shown in Figure 6 c) and d) and in Table 2. The lower site density here was chosen because on the plane where the singly coordinated group appears, various other groups are also present (doubly- and triply coordinated ones, which were not treated). The chosen site-density is often used for similarly undefined sorbents, for which precise contributions from different planes is not available.

Obtained results lead to the conclusion that the NWs surface is more acidic than surface of the NTs. As shown in Figure 6 a) and b) the  $\text{pH}_{\text{iep}}$  shifts to the higher values as ionic strength increases for both NWs and NTs. The shift of the  $\text{pH}_{\text{iep}}$  value to the basic region indicates a higher affinity for cation binding on the respective  $\text{TiO}_2$  surface. Ridley et al.<sup>10</sup> obtained the same results, i.e.  $\text{pH}_{\text{iep}}$  shifts to the higher pH values as the ionic strength increases due to the higher  $\text{Na}^+$  ion affinity for the  $\text{TiO}_2$  nanocrystalline anatase. Kormann et al.<sup>65</sup> determined that the  $\text{pH}_{\text{iep}}$  of the nanocrystalline anatase (diameter of the particles was less than 3 nm) is  $\text{pH}_{\text{iep}} = 5.1$ . The obtained values of the  $\text{pH}_{\text{iep}}$  for the NWs and NTs in this study are observed in more acidic pH region compared with nanocrystalline anatase<sup>65</sup> or macroscopic  $\text{TiO}_2$ .<sup>66</sup> Thermodynamic descriptions of the ion adsorption equilibrium constants can be considered within surface complexation models. The MUSIC model framework used for the determination of the surface protonation constants, give insights in the cation affinity for the surface of the NWs and NTs (Table 2). Calculated constants for the ion affinity of the NWs and NTs has shown that the  $\log K$  values for cations are higher than for anions which was also obtained in the work of Bourikas et al.<sup>64</sup>

Besides crystal phase, size is also one of the important factors that affect the relative reactivity/acidity of the investigated materials. Size distributions, i.e. length and diameters of the NWs and NTs are obtained from the HR-SEM (Figure 1 b), c), e) and f)) and HR-TEM measurements (Figure 2-3, e) and f)), as well as from Dynamic Light Scattering (DLS) measurements (Supporting Information Material, Figures S11 and S12). From the HR-SEM and the HR-TEM images it is clearly visible that the walls of NWs and NTs stick together, thus forming bundles due to high affinity toward self-assembly. Length distribution obtained from the HR-SEM measurements indicate that NTs are longer than NWs, while NWs are wider than NTs. Hydrodynamic diameter of both nanostructures was measured as a function of pH at different ionic strengths.

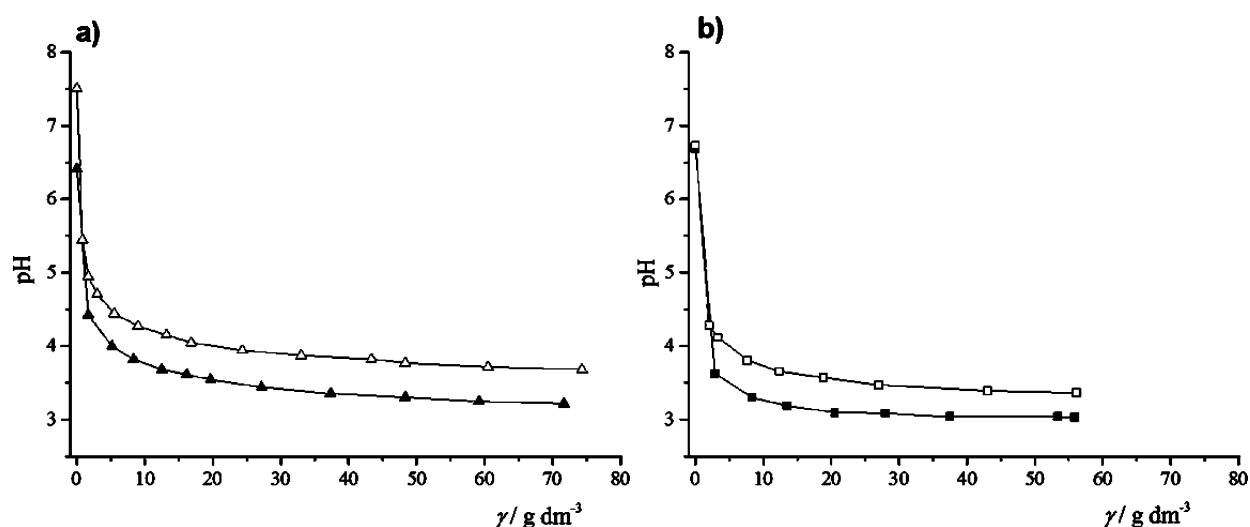


**Figure 7.** Potentiometric mass titration of TiO<sub>2</sub> nanomaterials in NaNO<sub>3</sub> aqueous electrolyte solution. a) NWs: ( $\Delta$ )  $I_{c,0} = 0.1$  mM, ( $\blacktriangle$ )  $I_{c,0} = 10$  mM; b) NTs: ( $\square$ )  $I_{c,0} = 0.1$  mM, ( $\blacksquare$ )  $I_{c,0} = 10$  mM.  $\theta = 25$  °C.

Although, a good agreement with electrokinetic data was obtained, the DLS results should be taken with care. One intrinsic problem of the DLS technique is that the obtained effective diameter is the size of the equivalent sphere, *i.e.* a spherical particle with the same diffusion coefficient as particles in question. In addition, suspensions for DLS measurements were prepared by ultrasound treatment which could result in fragmentation and breakage of the NWs and NTs. Therefore, strict conclusions on effect of the size on the  $\text{pH}_{\text{iep}}$  could not be drawn.

In Figure 7 the results of potentiometric mass titrations of the NWs and NTs samples starting with two initial ionic strengths,  $I_{c,0} = 0.1$  mM and  $I_{c,0} = 10$  mM are presented. When dry powder is added in the aqueous electrolyte solution, the pH of the suspension is changing due to release of protons from the  $\equiv\text{TiOH}$  surface groups. pH changes until it eventually achieves a constant value where further additions of the dry powder cause no change. The final pH,  $\text{pH}_{\infty}$  corresponds to the point of zero charge ( $\text{pH}_{\text{pzc}}$ ) in the samples that are extensively washed during the synthesis procedure so that all acidic and basic impurities are removed. At the  $\text{pH}_{\text{pzc}}$  the TiO<sub>2</sub> surface is uncharged because of an equal number of positive and negative active surface sites. Maximum mass concentration for the NWs was  $\approx 80$  g dm<sup>-3</sup> while for the NTs was  $\approx 60$  g dm<sup>-3</sup>. The points of zero charge for the both samples are given in Table 3.

As the ionic strength increases,  $\text{pH}_{\text{pzc}}$  shifts to lower pH for both NWs and NTs. The isoelectric point and point of zero charge of the NWs are in good agreement,  $3.1 < \text{pH}_{\text{iep}}(\text{pH}_{\text{pzc}}) < 3.7$ . On the other side, a discrepancy in the values of isoelectric point and point of zero charge of the NTs is observed. The

**Table 3.** Point of zero charge for NWs and NTs samples at two initial ionic strengths,  $I_{c,0} = 0.1$  mM and  $I_{c,0} = 10$  mM determined from potentiometric mass titrations.  $\Delta\text{pH}_{\text{pzc}} = \text{pH}_{\text{pzc}}(I_{c,0} = 10 \text{ mM}) - \text{pH}_{\text{pzc}}(I_{c,0} = 0.1 \text{ mM})$

TiO <sub>2</sub> nanomaterial	$\text{pH}_{\text{pzc}}$		$\Delta\text{pH}_{\text{pzc}}$
	$I_{c,0} = 0.1$ mM	$I_{c,0} = 10$ mM	
NWs	3.7	3.2	0.5
NTs	3.3	3.0	0.3

isoelectric point is in the range  $4.6 < \text{pH}_{\text{iep}} < 5.5$ , while the point of zero charge is observed in the range  $3.0 < \text{pH}_{\text{pzc}} < 3.3$ . This difference could be explained by the change in the stability of the NTs due to the mechanical treatment which is inevitable during the measurements performing. During the experiment the ultrasound is applied and it could cause the fragmentation of the NTs which could result in the loss of the tubular morphology<sup>58</sup> as shown by the atomic force microscopy, thus leading to significant decrease in the specific surface area. Another reason for the low point of the zero charge obtained from the potentiometric mass titration of the NTs is due to the kinetics of the ion-exchange. Baykin et al.<sup>40</sup> investigated the effect of the ion-exchange between NTs and lithium hydroxide on the kinetics and change in pH of the suspension. Their results have shown significant pH decrease of the NTs suspension after 60 min at mass concentration  $\gamma = 10$  g dm<sup>-3</sup>. The significant drop in the pH could be explained in the terms of kinetic regulation of the ion-exchange process. There are few processes during the ion-exchange: a) adsorption of metal ion from the bulk onto the surface of the NTs, b) transport of the metal ion inside the NTs to the ion-exchange centers and the reverse transport of protons, c) transport of protons from the inside of the NTs to the surface and d) releasing the proton from the surface of the NTs to the bulk which cause the significant pH decrease in the suspension of the NTs. The details can be found in the ref 40. In our study, the mass concentration was higher, so the effect of the pH decrease is more prominent.

The shift of the point of zero charge of the NWs and NTs to lower pH as the ionic strength increases is due to the higher affinity of cations for the TiO<sub>2</sub> nanomaterial surface compared to anions. The same evidence was obtained in the study of different TiO<sub>2</sub> surfaces (anatase, rutile and TiO<sub>2</sub> P25) where the affinity of the cations for the TiO<sub>2</sub> surface was higher than for the anions.<sup>23,26</sup>

Surface charge,  $\sigma_0$ , as shown in Figure 8, calculated from the potentiometric mass titrations using eq 3 is derived from interactions of surface hydroxyl groups with potential determining ions and that interaction depends on the pH as well as the ionic strength of the solution. The surface charge is higher for the NWs compared to NTs due to a significant difference in their specific surface area.

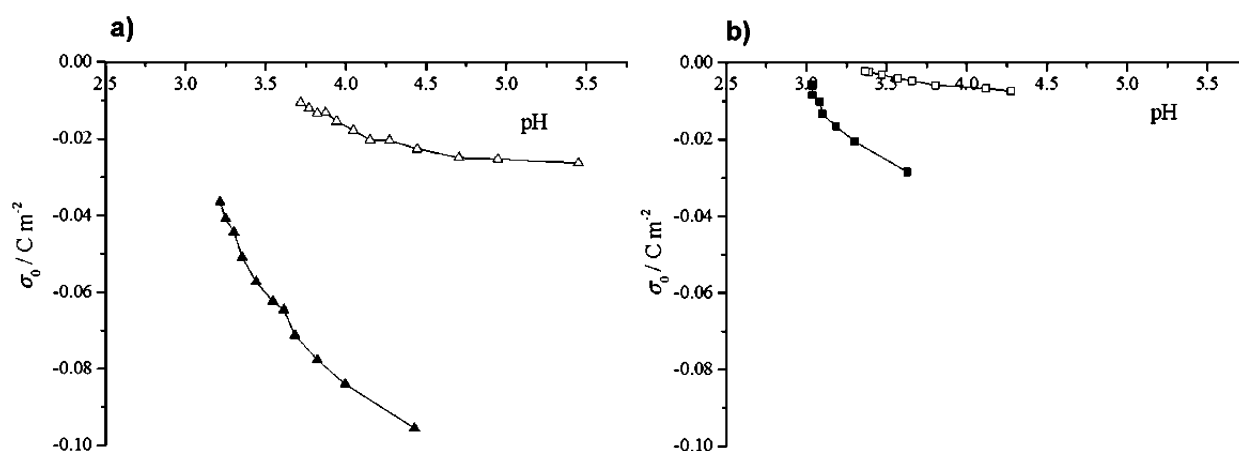


**Figure 8.** Surface charge determined from the potentiometric mass titration of TiO<sub>2</sub> nanomaterials in NaNO<sub>3</sub> aqueous electrolyte solution. a) NWs: (Δ)  $I_{c,0} = 0.1$  mM, (▲)  $I_{c,0} = 10$  mM; b) NTs: (□)  $I_{c,0} = 0.1$  mM, (■)  $I_{c,0} = 10$  mM.  $\vartheta = 25$  °C.

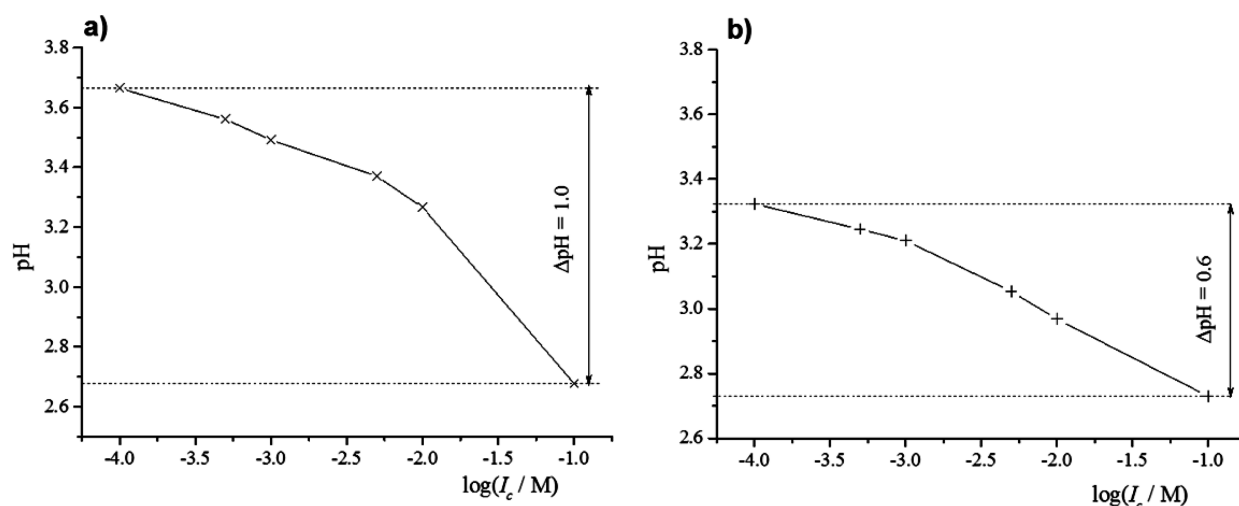


**Figure 9.** Potentiometric electrolyte titration of TiO<sub>2</sub> nanomaterials in NaNO<sub>3</sub> aqueous electrolyte solution. a) (x) NWs, b) (+) NTs. The initial ionic strength was  $I_{c,0} = 0.1$  mM and  $\vartheta = 25$  °C.

To confirm stronger affinity of cations for the NWs and NTs surfaces the potentiometric electrolyte titrations were performed. Potentiometric electrolyte titration of NWs or NTs in NaNO<sub>3</sub> aqueous electrolyte solution is presented in Figure 9.

Cations exhibit strong effect on the NWs and NTs surfaces as shown in Figure 9. An increase in the electrolyte concentration shifts the pH of a dense suspension to acidic pH region in the case of NWs and NTs compared to an initial pH of dense suspension,  $pH_{\infty}$ . Opposing to our expectations, the pH decrease is higher for the NWs than for NTs even though the specific surface area of the NTs is ten times higher. Obtained results could be explained with the availability of the NTs surface area to the solution, especially around the point of zero charge and high ionic strength where aggregation occurs and the specific surface area is reduced. The shift to lower pH is attributed to the preferential adsorption of cations on the NWs or NTs surfaces previously reported results.<sup>10,14,65,66</sup> The ionic strength has a significant effect on the lowering the pH of the NTs and NWs suspension. We believe that for the NWs the shift in  $pH_{iep}$  and the electrolyte effect in the electrolyte titration are to some extent related to the Na<sup>+</sup> ions association being much stronger than the NO<sub>3</sub><sup>-</sup> ion association this is also something that emerges from the paper of Bourikas et al.<sup>65</sup> The role of the cations has been shown in other TiO<sub>2</sub> systems, often

by molecular dynamics simulations. Work by Predota et al.<sup>67</sup> suggests that Na<sup>+</sup> ion “jumps” to the surface. This would mean that Na<sup>+</sup> ions indeed affect the surface potential. This has also been postulated for other surfaces in particular for hematite (001).<sup>68</sup> Besides ion-exchange process which takes part, we have mentioned already that the ultrasound treatment can affect the nanostructures. In the case of the NTs if ultrasound destroys part of the particles, inner surfaces could become exposed and then react in a different manner than when they are exposed to confined water. A simpler explanation would be that the electrokinetic potential measurements are only testing the outer surfaces, while titrations test in principle all the exposed surfaces. Thus, proton related reactions within the NTs would affect the potentiometric mass and electrolyte titrations but not the electrokinetic potentials.

The surface charge of TiO<sub>2</sub> nanomaterials is determined by the pH of the aqueous electrolyte solution and counterion adsorption. The active surface TiO<sub>2</sub> groups may be  $\equiv TiOH$ ,  $\equiv TiOH_2^+$  and  $\equiv TiO^-$  according to pH of the medium, i.e. acid–base properties of the metal oxide have significant contribution to the overall photocatalysis efficiency.<sup>69</sup>

Our investigation confirms stronger affinity of the cation for the TiO<sub>2</sub> NWs and NTs surface in comparison with the anions. Na<sup>+</sup> ions compensate surface charge of the  $\equiv TiO^-$  groups for

both NWs and NTs due to the attractive electrostatic forces. Additionally, the mesoporous morphology of the NTs enables exchange of the protons between the multilayered walls and cations from the suspension.

It is important to determine basic surface characteristics ( $\text{pH}_{\text{iep}}$ ,  $\text{pH}_{\text{pzc}}$ ) of the metal oxide under different pH values and the ionic strengths because most of the studies in the literature related to NWs and NTs photocatalysis deal with organic molecules and their adsorption onto a polar support, such as  $\text{TiO}_2$ , particularly in aqueous solution. This process will depend on the  $\text{TiO}_2$  acid–base surface properties. Since pH influences surface charge and surface potential, it can have a pronounced effect on the adsorption of an organic pollutant, which in turn, influences the efficiency of  $\text{TiO}_2$  in photocatalyzing its degradation. In addition, surface pH affects the energetics of the valence and conduction band, which further influences photocatalytic efficiency of the metal oxide. And last, organic pollutants present in waste waters can exhibit different speciation behavior at different pHs. They may remain uncharged, or change their charge depending on the pH of the waste waters. The surface pH and the ionic strength might serve as a tool for controlling the  $\text{TiO}_2$  nanomaterials surface speciation due to its amphoteric character. In this way, the application of the  $\text{TiO}_2$  nanomaterials as photocatalyst could be more effective.

This research reveals the importance of the acid–base surface properties, surface reactivity/acidity and utilization of the ionic strength as a means to control parameters that influence the adsorption characteristics of the metal oxide surface. We believe that the determination of surface charge as well as the surface pH is important and crucial for a better understanding of  $\text{TiO}_2$ 's photocatalytic properties in general, especially for one-dimensional  $\text{TiO}_2$  nanomaterials, NWs and NTs.

#### 4. CONCLUSIONS

This work presents a systematic study of the effects of the morphology, crystal phase and size on the surface properties of the  $\text{TiO}_2$  one-dimensional nanomaterials. We have correlated morphology, crystal phase and size of the NWs and NTs with the determined surface properties,  $\text{pH}_{\text{iep}}$  and  $\text{pH}_{\text{pzc}}$ . For the NWs, the isoelectric point is observed in more acidic region,  $3 < \text{pH}_{\text{iep}} < 4$ , while for the NTs the isoelectric point is observed in a mild acidic region,  $4 < \text{pH}_{\text{iep}} < 6$ . Surface protonation constants which further give insights into the surface charging behavior of the NWs and NTs were determined using the MUSIC model framework. The obtained surface protonation constants assign NWs as nanomaterial with higher surface acidity/reactivity than NTs.

Points of zero charge for NWs and NTs samples were determined from potentiometric mass titrations. Obtained results from the potentiometric mass titrations for the NWs are in good agreement with those determined from the electrokinetic measurements. On the other side, surface properties of the NTs, i.e.  $\text{pH}_{\text{iep}}$  and  $\text{pH}_{\text{pzc}}$  significantly differs. The discrepancy between  $\text{pH}_{\text{iep}}$  and  $\text{pH}_{\text{pzc}}$  of the NTs is explained in terms of the mechanical treatment and their stability. In the present work, we also report the effect of the ionic strength on the pH of NWs and NTs surface properties, surface reactivity/acidity. In general, our results point a strong cation effect, i.e. higher cation affinity for the  $\text{TiO}_2$  surface from electrokinetic measurements, potentiometric mass and electrolyte titrations. The isoelectric point shifts to higher pH, whereas the point of the zero charge shifts to the lower pH as the ionic strength

increase. Surface characteristics such as morphology, exposed crystal planes and active surface groups character clearly distinguish the surface reactivity/acidity for the NWs and NTs.

Detailed characterization of the surface characteristics such as morphology, exposed crystal planes, presence of the different surface groups as well as ion coordination of the nanosized NWs and NTs could contribute to better understanding of the surface behavior of the NWs and NTs and improve their application.

Furthermore, these findings emphasize the importance of the presence of common electrolyte, such as  $\text{NaNO}_3$ , which can influence surface pH, and in turn, overall photocatalytic activity and efficiency.

#### ■ ASSOCIATED CONTENT

##### Supporting Information

The Supporting Information is available free of charge on the ACS Publications website at DOI: 10.1021/acs.jpcc.5b02027.

Terms related with the charging of the metal oxide/aqueous electrolyte solution interface; Raman and FTIR spectra, as well as assignment of the observed bands; X-ray photoelectron spectroscopy measurements for the NWs and NTs; reproducibility of the electrokinetic measurements for the both NWs and NTs; and dynamic light scattering, i.e., size measurements, are presented (Figures S1–S12 and Tables S1–S5) (PDF)

#### ■ AUTHOR INFORMATION

##### Corresponding Authors

\*A.S.: tel, +385 (1) 4606130; e-mail, [aselmani@chem.pmf.hr](mailto:aselmani@chem.pmf.hr).

\*E.R.: tel, +49 (721) 608 24102; e-mail, [engelbert.redel@kit.edu](mailto:engelbert.redel@kit.edu).

##### Author Contributions

The manuscript was written through contributions of all authors. All authors gave given approval to the final version of the manuscript.

##### Notes

The authors declare no competing financial interest.

#### ■ ACKNOWLEDGMENTS

A.S. thank the Ministry of Science, Education and Sports of the Republic of Croatia (project No. 119-1191342-2961) for financial support. E.R. thanks the Alexander von Humboldt (AvH) Foundation as well as KIT and SMG for financial support and funding. I.D.M. acknowledges the Unity through Knowledge Fund, Croatia grant no. 17/13. H.D.G. gratefully acknowledges support of this research from the National Science Foundation (CHE-0514458), Corning, Inc., CUNY Center of Advance Technology in Photonics, supported by the New York State Science and Technology Foundation, and the PSC-BHE Grant Program of CUNY. The support and access to all facilities of the KNMF Laboratory for Microscopy and Spectroscopy at KIT is also acknowledged here. M.P. and M.W. thanks the Ministry of Science, Education and Sports of the Republic of Croatia and the DAAD agency in Germany (Croatian–German bilateral project) for their support. The authors would like to thank to A. Kendel (Division of Analytical Chemistry, Faculty of Science) for technical help with Raman scattering and FT-IR spectroscopy, L. Štajner (Division of materials chemistry, Ruđer Boković Institute) for help with the Brunauer–Emmett–Teller method, M. Zbačnik for the powder XRD measurements, and L. Schöttner (Institute for Function-

alized Interfaces, Karlsruhe Institute for Technology) for the XPS measurements and the interpretation of the data. We also thank to Assoc. Prof. T. Preočanin for valuable comments.

## REFERENCES

- (1) Bogue, R. Nanosensors: A Review of Recent Progress. *Sens. Rev.* **2009**, *29*, 310–315.
- (2) Garcia-Barriocanal, J.; Rivera-Calzada, A.; Varela, M.; Sefrioui, Z.; Diaz-Guillén, M. R.; Moreno, K. J.; Díaz-Guillén, J. A.; Iborra, J. E.; Fuentes, A. F.; Pennycook, et al. Tailoring Disorder and Dimensionality: Strategies for Improved Solid Oxide Fuel Cell Electrolytes. *ChemPhysChem* **2009**, *10*, 1003–1011.
- (3) Patzke, G. R.; Zhou, Y.; Kontic, R.; Conrad, F. Oxide Nanomaterials: Synthetic Developments, Mechanistic Studies and Technological Innovations. *Angew. Chem., Int. Ed.* **2011**, *50*, 826–859.
- (4) Yang, D. Y.; Zheng, Z. F.; Liu, H. W.; Zhu, H. Y.; Ke, X. B.; Xu, Y.; Wu, D.; Sun, Y. Layered Titanate Nanofibers as Efficient Adsorbents for Removal of Toxic Radioactive and Heavy Metal Ions from Water. *J. Phys. Chem. C* **2008**, *112*, 16275–16280.
- (5) Joo, J.; Kwon, S. G.; Yu, T.; Cho, M.; Lee, J.; Yoon, J.; Hyeon, T. Large-Scale Synthesis of the TiO<sub>2</sub> Nanorods Via Nonhydrolytic Sol-Gel Ester Elimination Reaction and Their Application to Photocatalytic Inactivation of E. Coli. *J. Phys. Chem. B* **2005**, *109*, 15297–15302.
- (6) Zhu, H.; Gao, X.; Lan, Y.; Song, D.; Xi, J.; Zhao, J. Hydrogen Titanate Nanofibers Covered with Anatase Nanocrystals: A Delicate Structure Achieved by the Wet Chemistry Reaction of the Titanate Nanofibers. *J. Am. Chem. Soc.* **2004**, *126*, 8380–8381.
- (7) Bavykin, D. V.; Friedrich, J. M.; Walsh, A. C. Protonated Titanates and TiO<sub>2</sub> Nanomaterials: Synthesis, Properties and Applications. *Adv. Mater.* **2006**, *18*, 2807–2824.
- (8) Chen, X.; Mao, S. S. Titanium Dioxide Nanomaterials: Synthesis, Properties, Modifications, and Applications. *Chem. Rev.* **2007**, *107*, 2891–2959.
- (9) Davis, J. A.; James, R. O.; Leckie, J. O. Surface Ionization and Complexation at the Oxide/Water Interface. *J. Colloid Interface Sci.* **1978**, *63*, 480–499.
- (10) Ridley, M. K.; Hackley, V. A.; Machesky, M. L. Characterization and Surface-Reactivity of Nanocrystalline Anatase in Aqueous Solutions. *Langmuir* **2006**, *22*, 10972–10982.
- (11) Rajh, T.; Chen, L. X.; Lukas, K.; Liu, T.; Thurnauer, M. C.; Tiede, D. M. Surface Restructuring of Nanoparticles: An Efficient Route for Ligand–Metal Oxide Crosstalk. *J. Phys. Chem. B* **2002**, *106*, 10543–10552.
- (12) Grover, I. S.; Singh, S.; Pal, B. The Preparation, Surface Structure, Zeta Potential, Surface Charge Density and Photocatalytic Activity Of TiO<sub>2</sub> Nanostructures of Different Shapes. *Appl. Surf. Sci.* **2013**, *280*, 366–372.
- (13) Suttiponparnit, K.; Jiang, J.; Sahu, M.; Suvachittanont, S.; Charinpanitkul, T.; Biswas, P. Role of Surface Area, Primary Particle Size, and Crystal Phase on Titanium Dioxide Nanoparticle Dispersion Properties. *Nanoscale Res. Lett.* **2011**, *6*, 27.
- (14) Ahmad, M. A.; Prelot, B.; Dufour, F.; Durupthy, O.; Razafitianamaharavo, A.; Douillard, J. M.; Chaneac, C.; Villieras, F.; Zajac, J. Influence of Morphology and Crystallinity on Surface Reactivity of Nanosized Anatase TiO<sub>2</sub> Studied by Adsorption Techniques. 2. Solid-Liquid Interface. *J. Phys. Chem. C* **2013**, *117*, 4459–4469.
- (15) Kinsinger, N. M.; Dudchenko, A.; Wong, A.; Kisailus, D. Synergistic Effect of pH in a Nanocrystalline Titania Photocatalyst. *ACS Appl. Mater. Interfaces* **2013**, *5*, 6247–6254.
- (16) Liu, W.; Sun, W.; Borthwick, A. G. L.; Ni, J. Comparison on Aggregation and Sedimentation of Titanium Dioxide, Titanate Nanotubes and Titanate Nanotubes-TiO<sub>2</sub>: Influence of pH, Ionic Strength and Natural Organic Matter. *Colloids Surf., A* **2013**, *434*, 319–328.
- (17) Wang, N.; Lin, H.; Li, J. B.; Yang, X. Z.; Chi, B. Electrophoretic Deposition and Optical Property of Titania Nanotubes Films. *Thin Solid Films* **2006**, *496*, 649–652.
- (18) Liang, H. C.; Li, X. Z.; Yang, Y. H.; Sze, K. H. Effects of Dissolved Oxygen, pH, and Anions on the 2,3-Dichlorophenol Degradation by Photocatalytic Reaction with Anodic TiO<sub>2</sub> Nanotube Films. *Chemosphere* **2008**, *73*, 805–812.
- (19) Sheng, G.; Dong, H.; Shen, R.; Li, Y. Microscopic Insights into the Temperature-Dependent Adsorption of Eu(III) onto Titanate Nanotubes Studied by FTIR, XPS, XAFS and Batch Technique. *Chem. Eng. J.* **2013**, *217*, 486–494.
- (20) Selmani, A.; Špadina, M. Unpublished results.
- (21) Shaw, D. J. *Introduction to Colloid & Surface Chemistry*; Butterworth-Heinemann/ Oxford, 1992; pp 190–197.
- (22) Preočanin, T.; Kallay, N. Application of Mass Titration to Determination of Surface Charge of Metal Oxides. *Croat. Chem. Acta* **1998**, *71*, 1117–1125.
- (23) Berube, Y. G.; De Bruyn, P. L. Adsorption at the Rutile-Solution Interface. II. Model of the Electrochemical Double Layer. *J. Colloid Interface Sci.* **1968**, *28*, 92–105.
- (24) Milonjić, S. K.; Čerović, Lj. Š.; Čokeša, D. M.; Zec, S. The Influence of Cationic Impurities in Silica on its Crystallization and Point of Zero Charge. *J. Colloid Interface Sci.* **2007**, *309*, 155–159.
- (25) Kovačević, D.; Preočanin, T.; Žalac, S.; Čop, A. Electrostatic Potentials at Solid/Liquid Interfaces. *Croat. Chem. Acta* **2007**, *80*, 287–301.
- (26) Sprycha, R. Surface Charge and Adsorption of Background Electrolyte Ions at Anatase/Electrolyte Interface. *J. Colloid Interface Sci.* **1984**, *102*, 173–185.
- (27) Machesky, M. L.; Wesolowski, D. J.; Palmer, D. A.; Ichiro-Hayashi, K. Potentiometric Titrations of Rutile Suspensions at 250 °C. *J. Colloid Interface Sci.* **1998**, *200*, 298–309.
- (28) Bullard, J. W.; Cima, M. J. Orientation Dependence of the Isoelectric Point of TiO<sub>2</sub> (Rutile) Surfaces. *Langmuir* **2006**, *22*, 10264–10271.
- (29) Fitts, J. P.; Machesky, M. L.; Wesolowski, D. J.; Shang, X.; Kubicki, J. D.; Flynn, G. W.; Heinz, T. F.; Eiseenthal, K. B. Second-Harmonic Generation and Theoretical Studies of Protonation at the Water/A-TiO<sub>2</sub> (110) Interface. *Chem. Phys. Lett.* **2005**, *411*, 399–403.
- (30) Kasuga, T.; Hiramatsu, M.; Hosono, A.; Sekino, T.; Niihara, K. Formation of Titanium Oxide Nanotube. *Langmuir* **1998**, *14*, 3160–3163.
- (31) Nečas, D.; Klapetek, P. Gwyddion: An Open-Source Software for SPM Data Analysis. *Cent. Eur. J. Phys.* **2012**, *10*, 181–188.
- (32) *Philips X'Pert Graphics & Identify 1.3e*; Philips Analytical B.V.: Amsterdam, Netherlands, 2001.
- (33) Lützenkirchen, J.; Preočanin, T.; Kovačević, D.; Tomišić, V.; Lövgren, L.; Kallay, N. Potentiometric Titrations as a Tool for Surface Charge Determinations. *Croat. Chem. Acta* **2012**, *85*, 391–417.
- (34) Preočanin, T.; Kallay, N. Point of Zero Charge and Surface Charge Density of TiO<sub>2</sub> in Aqueous Electrolyte Solution as Obtained by Potentiometric Mass Titration. *Croat. Chem. Acta* **2006**, *79*, 95–106.
- (35) Lide, D. R. *CRC Handbook of Chemistry and Physics*; CRC Press: Boca Raton: FL, 2007; pp 1274.
- (36) Ridley, M. K.; Hiemstra, T.; van Riemsdijk, W. H.; Machesky, M. L. Inner-Sphere Complexation of Cations at the Rutile–Water Interface: A Concise Surface Structural Interpretation with the CD and MUSIC Model. *Geochim. Cosmochim. Acta* **2009**, *73*, 1841–1856.
- (37) Machesky, M. L.; Wesolowski, D. J.; Palmer, D. A.; Ridley, M. K. On the Temperature Dependence of Intrinsic Surface Protonation Equilibrium Constants: An Extension of the Revised MUSIC Model. *J. Colloid Interface Sci.* **2001**, *239*, 314–327.
- (38) Darányi, M.; Kukovecz, Á.; Horváth, E.; Kónya, Z.; Kiricsi, I. Fine Tuning The Coverage of a Titanate Nanowire Layer on a Glass Substrate. *Chem. Phys. Lett.* **2008**, *460*, 191–195.
- (39) Suzuki, Y.; Pavasupree, S.; Yoshikawa, S.; Kawahata, R. Natural Rutile-Derived Titanate Nanofibers Prepared by Direct Hydrothermal Processing. *J. Mater. Res.* **2005**, *20*, 1063–1070.

- (40) Bavykin, D. V.; Walsh, F. C. Kinetics of Alkali Metal Ion Exchange into Nanotubular and Nanofibrous Titanates. *J. Phys. Chem. C* **2007**, *111*, 14644–14651.
- (41) Xiang, G.; Wang, J. G.; Li, J.; Zhuang, J.; Wang, X. Surface-Specific Interaction by Structure-Match Confined Pure High-Energy Facet of Unstable TiO<sub>2</sub>(B) Polymorph. *Sci. Rep.* **2013**, *3*, 1411.
- (42) Li, J.; Wan, W.; Zhou, H.; Li, J.; Xu, D. Hydrothermal Synthesis of TiO<sub>2</sub>(B) Nanowires with Ultrahigh Surface Area and their Fast Charging and Discharging Properties in Li-ion Batteries. *Chem. Commun.* **2011**, *47*, 3439–3441.
- (43) Bavykin, D. V.; Walsh, F. C. *Titanate and Titania Nanotubes: Synthesis, Properties and Application*; Royal Chemical Society: Cambridge: UK, 2010; pp 50–56.
- (44) Qian, L.; Du, Z. L.; Yang, S. Y.; Jin, Z. S. Raman Study of Titania Nanotube by Soft Chemical Process. *J. Mol. Struct.* **2005**, *749*, 103–107.
- (45) Zhang, Y. H.; Xiao, P.; Zhou, X. Y.; Liu, D. W.; Cao, G. Z. Carbon Monoxide Annealed TiO<sub>2</sub> Nanotube Array Electrodes for Efficient Biosensor Applications. *J. Mater. Chem.* **2009**, *19*, 948–953.
- (46) Cong, Y.; Xiao, L.; Zhang. Preparation and Characterization of Nitrogen-Doped TiO<sub>2</sub> Photocatalyst in Different Acid Environments. *Res. Chem. Intermed.* **2006**, *32*, 717–724.
- (47) Pu, P.; Cachet, H.; Laidani, N.; Sutter, E. M. M. Influence of pH on Surface States Behaviour in TiO<sub>2</sub> Nanotubes. *J. Phys. Chem. C* **2012**, *116*, 22139–22148.
- (48) Burda, C.; Lou, Y.; Chen, X. Enhanced Nitrogen Doping in TiO<sub>2</sub> Nanoparticles. *Nano Lett.* **2003**, *3*, 1049–1051.
- (49) Liu, W.; Wang, T.; Borthwick, A. G. L.; Wang, Y.; Yin, X.; Li, X.; Ni, J. Adsorption of Pb<sup>2+</sup>, Cd<sup>2+</sup>, Cu<sup>2+</sup> and Cr<sup>3+</sup> onto Titanate Nanotubes: Competition and Effect of Inorganic Ions. *Sci. Total Environ.* **2013**, *456–457*, 171–180.
- (50) Armstrong, A. R.; Armstrong, G.; Canales, J.; Bruce, P. G. TiO<sub>2</sub> (B) Nanowires. *Angew. Chem., Int. Ed.* **2004**, *43*, 2286–2288.
- (51) Ben Yahia, M.; Lemoigno, F.; Beuvier, T.; Filhol, J. S.; Richard-Plouet, M.; Brohan, L.; Doublet, M. L. Updated references for the Structural, Electronic, and Vibrational Properties of TiO<sub>2</sub>(B) Bulk Using First-Principles Density Functional Theory Calculations. *J. Chem. Phys.* **2009**, *130*, 204501–204511.
- (52) Gajović, A.; Frišćić, I.; Plodinec, M.; Iveković, D. High Temperature Raman Spectroscopy of Titanate Nanotubes. *J. Mol. Struct.* **2009**, *924–926*, 183–191.
- (53) Kesselman, J. M.; Weres, O.; Lewis, N. S.; Hoffmann, M. R. Electrochemical Production of Hydroxyl Radical at Polycrystalline Nb-doped TiO<sub>2</sub> Electrodes and Estimation of the Partitioning Between Hydroxyl Radical and Direct Hole Oxidation Pathways. *J. Phys. Chem. B* **1997**, *101*, 2637–2643.
- (54) Turchi, C. S.; Ollis, D. F. Photocatalytic Degradation of Organic Water Contaminants: Mechanisms Involving Hydroxyl Radical Attack. *J. Catal.* **1990**, *122*, 178–192.
- (55) Eremia, S. A. V.; Chevrier-Lucia, D.; Radu, G. L.; Marty, J. L. Optimization of Hydroxyl Radical Formation Using TiO<sub>2</sub> as Photocatalyst by Response Surface Methodology. *Talanta* **2008**, *77*, 858–862.
- (56) Stumm, W.; Hohl, H.; Dalang, F. Interaction of Metal Ions with Hydrous Oxide Surfaces. *Croat. Chem. Acta* **1976**, *48*, 491–504.
- (57) Sposito, G. On Points of Zero Charge. *Environ. Sci. Technol.* **1999**, *33*, 208–208.
- (58) Bavykin, D. V.; Walsh, F. C. *Titanate and Titania Nanotubes: Synthesis, Properties and Application*; Royal Chemical Society: Cambridge: UK, 2010; pp 7–8.
- (59) Hiemstra, T.; Van Riemsdijk, W. H. A Surface Structural Approach to Ion Adsorption: The Charge Distribution (CD) Model. *J. Colloid Interface Sci.* **1996**, *179*, 488–508.
- (60) Hiemstra, T.; Venema, P.; Van Riemsdijk, W. H. Intrinsic Proton Affinity of Reactive Surface Groups of Metal (Hydr)oxide: The Bond Valence Principle. *J. Colloid Interface Sci.* **1996**, *184*, 680–692.
- (61) Borghi, F.; Vyas, V.; Podestà, A.; Milani, P. Nanoscale Roughness and Morphology Affect the Isoelectric Point of Titania Surfaces. *PLoS One* **2013**, *8*, e68655–9.
- (62) Gateshki, M.; Peng, L.-M.; Chupas, P.; Petkov, V. Structure of Nanosized Materials by High-Energy X-Ray Diffraction: Study of Titanate Nanotubes. *Z. Kristallogr.* **2007**, *222*, 612–616.
- (63) Feist, T. P.; Davies, P. K. The Soft Chemical Synthesis of TiO<sub>2</sub> (B) from Layered Titanates. *J. Solid State Chem.* **1992**, *101*, 275–295.
- (64) Dzombak, D. A.; Morel, F. M. M. *Surface Complexation Modeling: Hydrous Ferric Oxide*; John Wiley & Sons: New York USA, 1990.
- (65) Bourikas, K.; Hiemstra, T.; Van Riemsdijk, W. H. Ion Pair Formation and Primary Charging Behavior of Titanium Oxide (Anatase and Rutile). *Langmuir* **2001**, *17*, 749–756.
- (66) Kormann, C.; Bahnemann, D. W.; Hoffmann, M. R. Preparation and Characterization of Quantum-Size Titanium Dioxide. *J. Phys. Chem.* **1988**, *92*, 5196–5201.
- (67) Předota, M.; Zhang, Z.; Fenter, P.; Wesolowski, D. J.; Cummings, P. T. Electric Double Layer at the Rutile (110) Surface. 2. Adsorption of Ions from Molecular Dynamics and X-ray Experiments. *J. Phys. Chem. B* **2004**, *108*, 12061–12072.
- (68) Lützenkirchen, J.; Heberling, F.; Šupljika, F.; Preočanin, T.; Kallay, N.; Johann, F.; Weisser, L.; Eng, P. J. Structure-Charge Relationship—the Case of Hematite (001). *Faraday Discuss.* **2015**, *180*, 55–79.
- (69) Bahnemann, D. W.; Cunningham, J.; Fox, M. A.; Pelizzetti, E.; Pichat, P.; Serpone, N. Photocatalytic Treatment of Waters. In *Aquatic Surface Photochemistry*; Zepp, R. G., Heltz, G. L., Crosby, D. G., Eds.; Lewis Publishers: Boca Raton, FL, 1994; pp 261–316.